

Columbia Astrophysics Laboratory	XMM-RGS	Doc.: RGS-COL-CAL-97002 Page: 1 Auth.: Joshua Spodek Date: February 1, 1997
---	----------------	--

Measurement of Single Grating Scatter at the Nevis Longbeam Facility

Document title:	Single Grating Scattering Measurement
Document version:	1
Distribution:	
SRON:	J.W. den Herder A. Brinkman P. de Korte H. Aarts
Columbia:	S. Kahn F. Paerels A. Rasmussen J. Spodek J. Cottam
PSI:	K. Thomsen
MSSL:	G. Branduardi-Raymont
ESTEC:	C. Erd P. Videler G. Vacanti

Introduction

This paper presents the method of analysis of the single grating scattering measurements conducted at the longbeam facility at Columbia's Nevis Laboratories. At present, over 150 gratings have been measured, and measurement continues at a rate of about 15 gratings per six-day week. We present first the underlying theory for scattering, then the procedure to test the theory and measure the grating properties, and finally the results of those measurements for single gratings as well as composite averages.

All the experimental results mentioned in this paper, updated as the measurements continue, are available at <http://astro1.nevis.columbia.edu/xmm>, under 'scattering data'.

Single Grating Scattering Theory

The schematic grating surface in figure 1 displays the relevant physical quantities of a blazed grating. The photon, of wavenumber $k = 2\pi/\lambda$, is incident on the grating with angle α and is diffracted with dispersion angle β . The blaze angle is δ and the graze angle relative to the local blazed grating surface is γ .

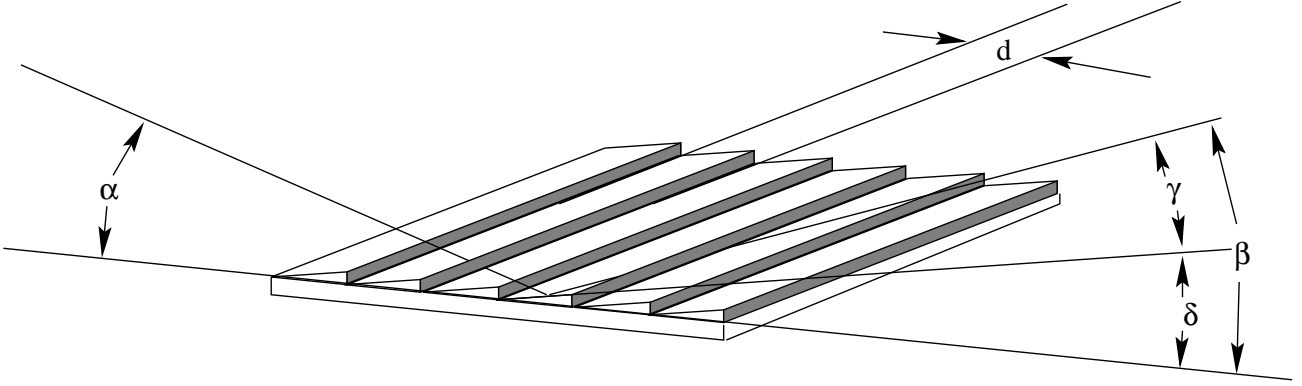


Figure 1: Schematic of the grating surface illustrating the incident and reflected angles relative to the macroscopic grating surface (α and β) and the reflected angle relative to the local, blazed surface (γ). Also the blaze angle, δ , is shown. All angles are $\sim 1^\circ$.

Line broadening due to scattering is calculated by scalar diffraction theory. This application is a new original calculation, which will soon be submitted for publication together with its experimental verification. Here we merely quote the results. The line profile at spectral order m —i.e., the relative efficiency, $d\eta_m$, for diffraction into the angular interval $\beta \rightarrow \beta + d\beta$ —is given by:

$$\frac{1}{\eta_m} \frac{d\eta_m}{d\beta} = \frac{(\sin \alpha + \sin \beta)^4}{(\sin \alpha + \sin \beta_m)^2} \sin \beta_m k^3 W(p), \quad (1)$$

where η_m is the total efficiency for diffraction in the m^{th} order, $W(p)$ is the surface power density spectrum of surface irregularities, β_m is the angle which satisfies the dispersion equation for spectral order m , and

$$W(p) = \frac{1}{2L} \frac{1}{2\pi} \left| \int_{-L}^L dx e^{ipx} \zeta(x) \right|^2.$$

Here $p = k(\cos \beta_m - \cos \beta)$ and $\zeta(x)$ is the height of the grating relative to a perfect blazed grating surface.

The integral of (1) gives the total integrated scatter (*TIS*), the fraction of light scattered out of the m^{th} order of the diffracted beam. This integral is approximately:

$$TIS = k^2 \sigma^2 (\sin \alpha + \sin \beta)^2. \quad (2)$$

where the rms height, σ , is given by:

$$\begin{aligned} \sigma^2 &= \frac{1}{2L} \int_{-L}^L dx |\zeta(x)|^2 \\ &= \int_{-\infty}^{\infty} dp W(p). \end{aligned}$$

Columbia Astrophysics Laboratory	XMM-RGS	Doc.: RGS-COL-CAL-97002 Page: 3 Auth.: Joshua Spodek Date: February 1, 1997
---	----------------	--

It is assumed that the surface deviations are characterized by a correlation length of surface deviations, l . This length, in turn, determines the angular width, $\delta\beta$, of the scattering profile. For a Gaussian distribution in $W(p)$, l and $\delta\beta$ are related by

$$\delta\beta = \frac{1}{\sqrt{2} k \sin \beta_m l}. \quad (3)$$

The dependence is similar for other distributions as well (Lorentzian, etc...).

Expressions (1) and (2) are valid in the small amplitude limit, where $\lambda \gg \sigma \sin \alpha$, and at small deflection angles of the surface relative to the critical graze angle for reflection ($\delta \sim \sigma/l$).

The predicted line profile, LP , at order $m \leq 0$ is a convolution of the throughbeam and the scattering model, SM , which is a sum of the scattered part and a perfectly diffracted part. When the beam passes undeflected to the detector the line profile is identical to the throughbeam, which may be considered as the case where $\zeta(x) \equiv 0$ and the scattering model is a delta function.

$$SM(\sigma, l) = \frac{1}{\eta_m} \frac{d\eta_m}{d\beta} + (1 - TIS) \times \delta(\beta - \beta_m) \quad (4)$$

$$LP = I_o * SM_m(\sigma, l), \quad (5)$$

where $*$ denotes convolution over β . LP depends on σ and l through $W(p)$.

The dependence on scattering properties of the gratings is contained in $W(p)$, while the rest of the RHS of (1) predicts how the scattering scales with order, energy, and incident angle. $W(p)$ is generally well represented by an analytic distribution parametrized by σ and l . In practice we use Gaussian distributions, which appear to work fairly well. According to the theory, once $W(p)$ is known for a grating, the scattering can be accurately predicted for any angle, energy, or incident angle.

Procedure

Experiment Description

Equations (4) and (5) suggest how to determine the grating's physical properties. Measuring the undeflected beam determines I_o . I_o can be analytically convolved with the scattering model in terms of the scattering parameters, σ and l , and then fitted to the line profile of diffracted orders to determine the best fit scattering parameters.

The theory predicts how the scattering should scale with order, energy, and incident angle. Equation (2) predicts how the fraction of scattered light, TIS , should increase with energy, through k , incident angle, α , and order, through β_m . Equation (3) predicts how the width of the scattered profile, $\delta\beta$, should decrease with increasing energy, through k and order, through β_m .

This section describes the tools and techniques used to determine the grating properties as indicated above.

Apparatus

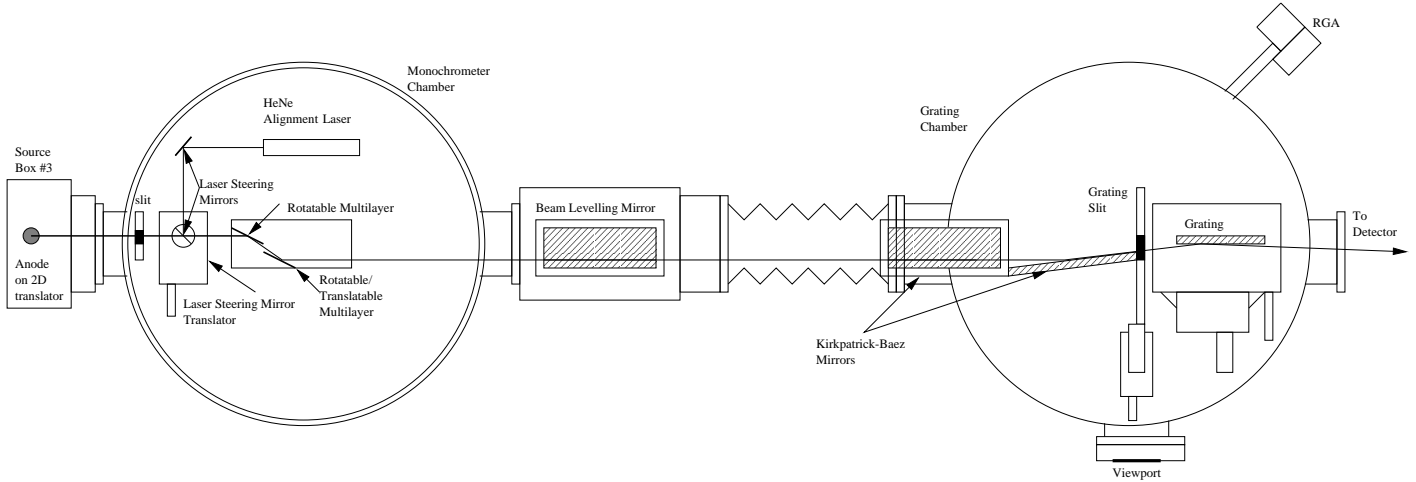


Figure 2: A schematic of the calibration facility at Nevis Laboratories. Not shown is the beam arm and detector chamber housing the detector 6.7 meters to the right (downstream) of the grating.

Figure 2 shows a schematic of the longbeam X-ray testing facility at Columbia University’s Nevis Labs. It features a changeable anode water-cooled electron impact source at left, producing an X-ray beam moving downstream to the right with a spectrum characteristic to the anode. Spectral lines are then isolated using a double multilayer tunable monochrometer. The beam is focused (focal length = 7.5 meters) using a pair of Kirkpatrick-Baez mirrors. The test grating lies downstream of the focusing optics on a rotatable, translatable stage, typically in the Electro-Optical Bread-Board (EOBB) six grating flight-representative mount. Downstream from the grating a pair of detectors—a proportional counter for efficiency measurements and an imaging multichannel plate for resolution measurements—lie at the end of a movable beam arm, not pictured in the schematic.

Figure 3 shows typical images from the multichannel plate (MCP) detector. The MCP is 38 mm (\approx 1200 arcsec) in diameter. A horizontal region including the slit is integrated over the vertical direction to create the foreground histogram. A pair of regions above and below the slit in each image is integrated to create the background. The background histogram is renormalized by ratio of area to foreground and subtracted from the foreground, creating the data sets plotted in later figures of this paper.

Fitting

The fitting procedure used to produce plots such as figure 4 requires some description. The RHS of equation (5), when solved analytically, can be written out as an expression in terms of the parameters of the throughbeam (I_o) and $W(p)$. Solving (5) analytically requires choosing explicit forms for $W(p)$ and I_o . These forms should adequately describe each term and be simply convolved together—as

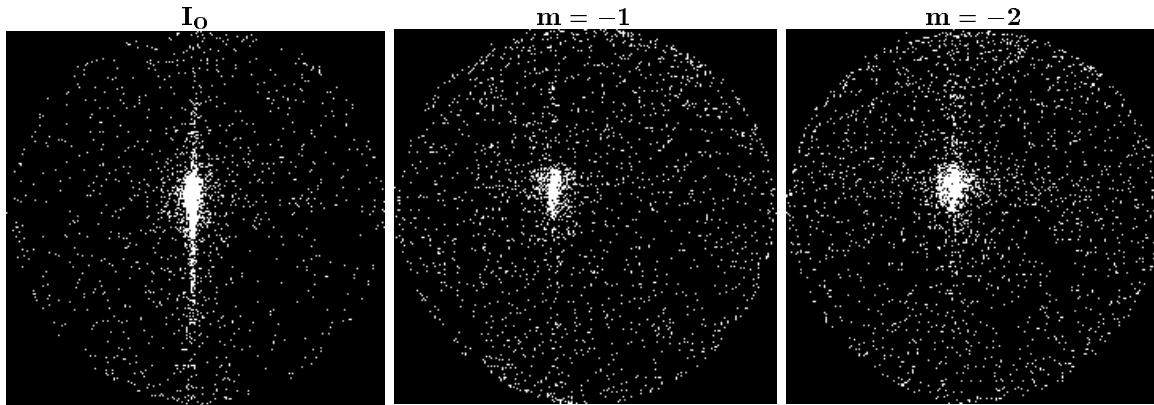


Figure 3: Images from the multichannel plate detector: A throughbeam, a first (inside) order, and a second (inside) order. These images were taken at $\text{AlK}\alpha$, incident angle $\alpha = 1.577^\circ$, and exposure times 50 - 100 sec. The circles are 38 mm in diameter and the dispersion is in the horizontal direction. The regions above and below the spots were used to subtract background.

mentioned above, we used Gaussians.

To find σ and l for a given data set, the corresponding throughbeam should be fit as well as possible. The top curve(s), labelled I_0 , on each figure are the throughbeams for the lower curves and are fitted with four Gaussians. Once fitted, the throughbeam parameters are fixed in the subsequent fitting of the diffracted orders. The lower curve(s), all diffracted orders, are fitted with LP , the convolution of the already fitted throughbeam and scattering model, parametrized by σ and l . The fitted curve is recentered and renormalized for each data set, but σ and l , physical properties of the grating, are constrained to be the same for all the fitted orders. The recentering, renormalization, and parameter fitting to the diffracted orders is done simultaneously.

Testing the Theory

Before measuring a large number of gratings we tested the theory on a small subset of gratings by comparing the theory's scaling predictions against measurement. Figure 4 shows the results of testing a grating over a range of energy— $E_{\text{Al K}} = 1.486$ keV, $E_{\text{Cu L}} = 0.929$ keV—and orders— $m = 0, -1, -2$.

Note that the scattering model predicts the scaling of the scattering as the order, energy, and incident angle change. The increase of the fraction of scattered light and the contraction of the core due to these changes is not fitted, but is correctly predicted by the model in equations (2) and (3). It is clear that the theory provides a reasonable description of the observed behavior.

The $\text{Al K}\alpha$ line has a complex of satellite lines which is well resolved in higher order on the TOT grating. This effect is well understood and unrelated to the scattering. Exposures with lower count rates, usually higher order or Cu lines, can be seen to show background effects closer to the core.

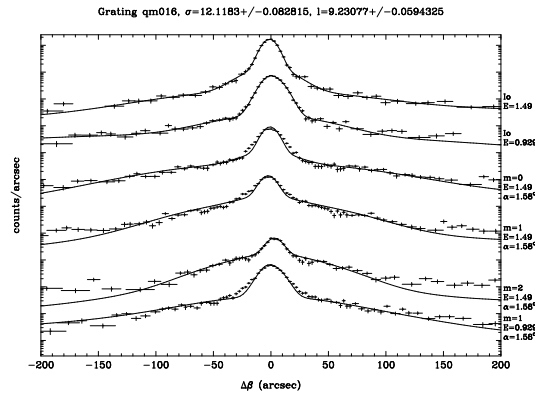


Figure 4: A series of line profiles from grating 016, used in the qualification model. The top two sets of the plot are throughbeams (I_0) and are fitted independently with four Gaussians. The lower sets are diffracted orders. Simultaneously, each diffracted order set is recentered and renormalized while all are fitted with σ and l .

Experimental Results

Having verified the basic predictions of the theory, we undertook our program of testing all the gratings. Of the anodes available, only Aluminum offered a sufficiently narrow line width and an adequate count rate to test a large number of gratings. Each grating tested has an image taken at $m = 0$ and one out of six (one per EOB load) has an additional image taken at $m = -2$.

Figure 5 shows the result of a typical measurement. This plot, in fact, derives from the raw data shown in figure 3 (in which only one of the two throughbeam images was displayed, for brevity). The data was reduced in the manner above. Note that two throughbeams were used to ensure against a change in the throughbeam in the time between when the first throughbeam was taken and the second order image was taken. As indicated, the results for this measurement were:

$$\begin{aligned}\sigma_{\text{fm}280} &= (13.8 \pm 0.3) \text{ \AA} \\ l_{\text{fm}280} &= (10.1 \pm 0.2) \mu\text{m}\end{aligned}$$

Figure 6 shows histograms of the scattering parameters for all 169 gratings tested as of this writing. The averages for all gratings are:

$$\begin{aligned}\sigma_{\text{ave}} &= (14.0 \pm 2.5) \text{ \AA} \\ l_{\text{ave}} &= (10.8 \pm 3.6) \mu\text{m}\end{aligned}$$

In order to test whether the gratings' scattering parameters changed as the replication process used more mature or later generation masters, figure 7 shows the evolution in time of the scattering

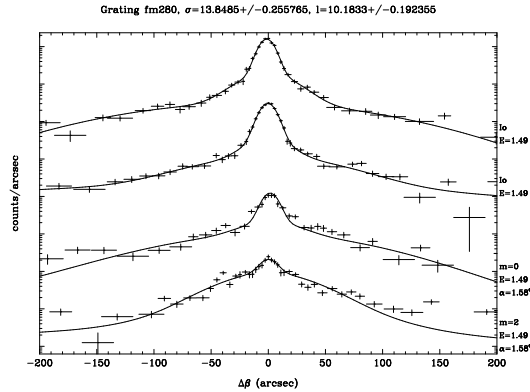


Figure 5: Typical results from the testing of a single grating. The data for this grating were measured over two orders (with a throughbeam measurement taken before each diffracted order measurement) and fitted simultaneously for the scattering parameters as described in the text. One sixth of the gratings were measured over two orders, the rest over one order only.

parameters. The date on the horizontal axis is the date of testing, which approximates the date of production, which approximates the genealogy of production. Therefore these graphs are only very rough indicators of any changes in scattering parameters with genealogy. In any case, no obvious trends are present.

Qualification Model Results: Panter

Testing of the entire RGS, as opposed to single gratings, was performed at the Panter X-ray testing facility near Munich. The larger Panter facility featured significantly higher luminosity, providing the opportunity to measure profiles at higher energies and orders than the Nevis longbeam could. In particular, scattering data for the qualification model (42 gratings in flight representative positions) were taken for:

Line	Energy (keV)	Orders
Si _{Kα}	1.74	-1,...,-4
Al _{Kα}	1.486	0,...,-3
Mg _{Kα}	1.25	0,...,-4
Cu _{Lα}	0.929	0,...,-2
O _{Kα}	0.526	0,...,-2

The scattering model is valid for $TIS \ll 1$, but equation (2) shows that TIS increases quadratically with energy and approximately quadratically with dispersion angle. The Panter data extend beyond where the above theory applies. Naive application of equation (2) unphysically predicts over 100% scattering for Si fourth order, whereas the data retain a well-defined core. Columbia's raytrace of the

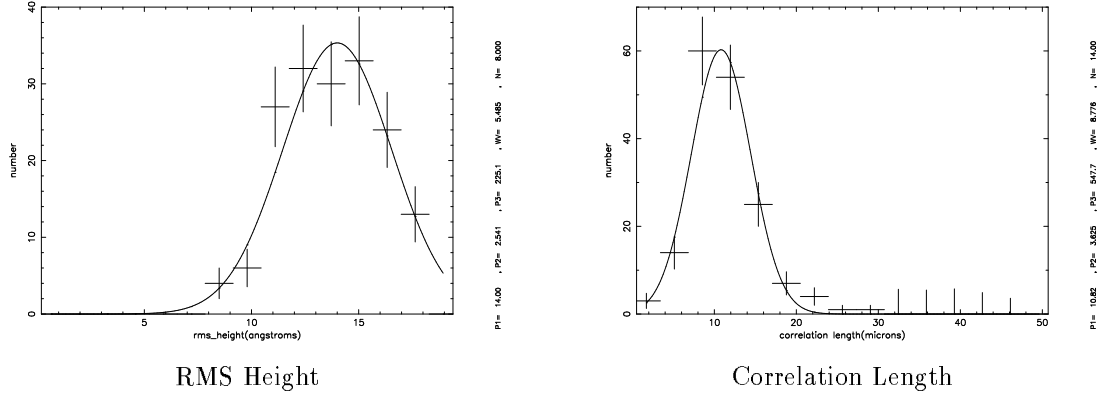


Figure 6: Histograms of the measured rms heights (σ) and correlation lengths (l) for all 169 gratings measured so far.

RGS predicted scattering using equation (2). Figure 8 shows that this prediction, valid at low dispersion angle, vastly overestimates the fraction of scattered light at higher orders. TIS must saturate at some point and approach 1 asymptotically.

Based on the ansatz that the scattering theory for a single grating should apply to the entire array of gratings in a similar way, we analyzed the Panter data in the manner described above for single gratings. Since the Panter data included no throughbeam, we approximated the throughbeam with a profile from a raytrace simulation with no scattering. Figure 9 shows three orders of Panter measurements analyzed this way. The best fit σ_{eff} , l_{eff} , and TIS_{eff} are indicated in the figure.

Figure 10 shows the total integrated scatter results from fitting the three highest energy ($\text{Si}_{K\alpha}$, $\text{Al}_{K\alpha}$, and $\text{Mg}_{K\alpha}$) Panter runs. Equation (2) predicts a straight line in this graph, passing through 100% total integrated scatter not much past $\text{Si}_{K\alpha}$, $m = -4$. The fitted curve is an ad-hoc function,

$$TIS = 1 - \frac{2}{e^{2k^2\sigma_{\text{eff}}^2(\sin\alpha + \sin\beta)^2} + 1}, \quad (6)$$

which displays the right limiting behavior. The value of the fitted parameter in this graph is $\sigma_{\text{eff}} = 11.62 \text{ \AA}$. Equation (2) was replaced in the Columbia raytrace with equation (6). When the raytrace was rerun with the new equation, figure 11 was obtained.

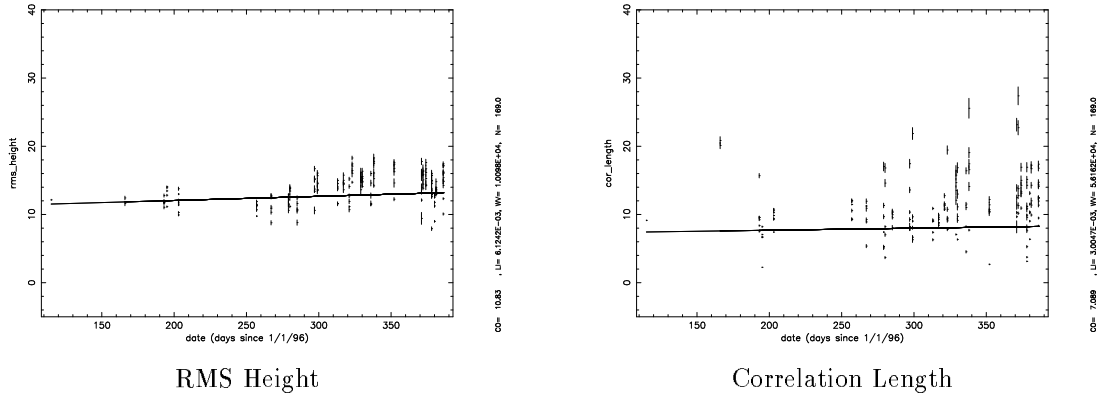


Figure 7: Time evolution of scattering parameters over time. Note that the horizontal axis—the date of grating testing—is only a very rough approximation of the grating genealogy.

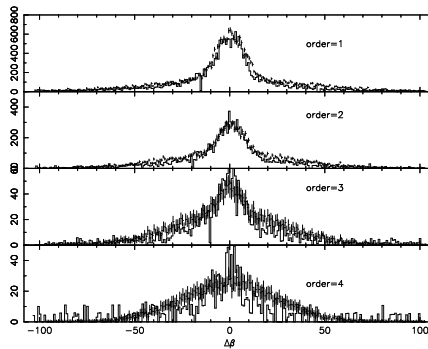
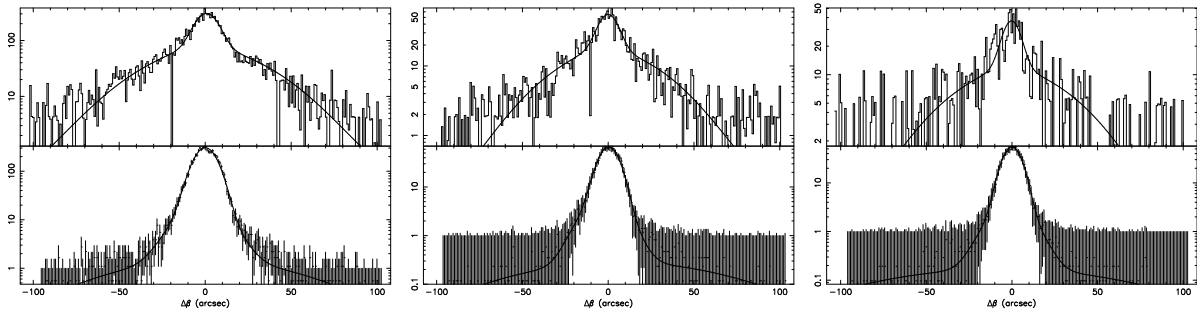


Figure 8: Profiles of Panter measurements of four orders at Si K_α (solid line) overlaid with simulations performed by the Columbia RGS raytrace. Note that the simulation vastly overpredicts the fraction of light scattered in $m = -3, -4$.



$\sigma_{\text{eff}} = (10.68 \pm 0.01)\text{\AA}$	$\sigma_{\text{eff}} = (10.49 \pm 0.04)\text{\AA}$	$\sigma_{\text{eff}} = (10.11 \pm 0.04)\text{\AA}$
$l_{\text{eff}} = (11.14 \pm 0.04)\mu\text{m}$	$l_{\text{eff}} = (10.2 \pm 0.2)\mu\text{m}$	$l_{\text{eff}} = (7.8 \pm 0.2)\mu\text{m}$
$TIS_{\text{eff}} = 0.547 \pm 0.001$	$TIS_{\text{eff}} = 0.645 \pm 0.004$	$TIS_{\text{eff}} = 0.704 \pm 0.005$

Figure 9: Three sets of Panter measurements analyzed to find σ_{eff} , l_{eff} , and TIS_{eff} for the Qualification Model. The lower data set in each plot is the result of a simulation with no grating scatter. Its parameters are fixed before convolving with the scattering model and fitting to the scattered data. The upper data set in each plot is the Panter data.

Total Integrated Scatter

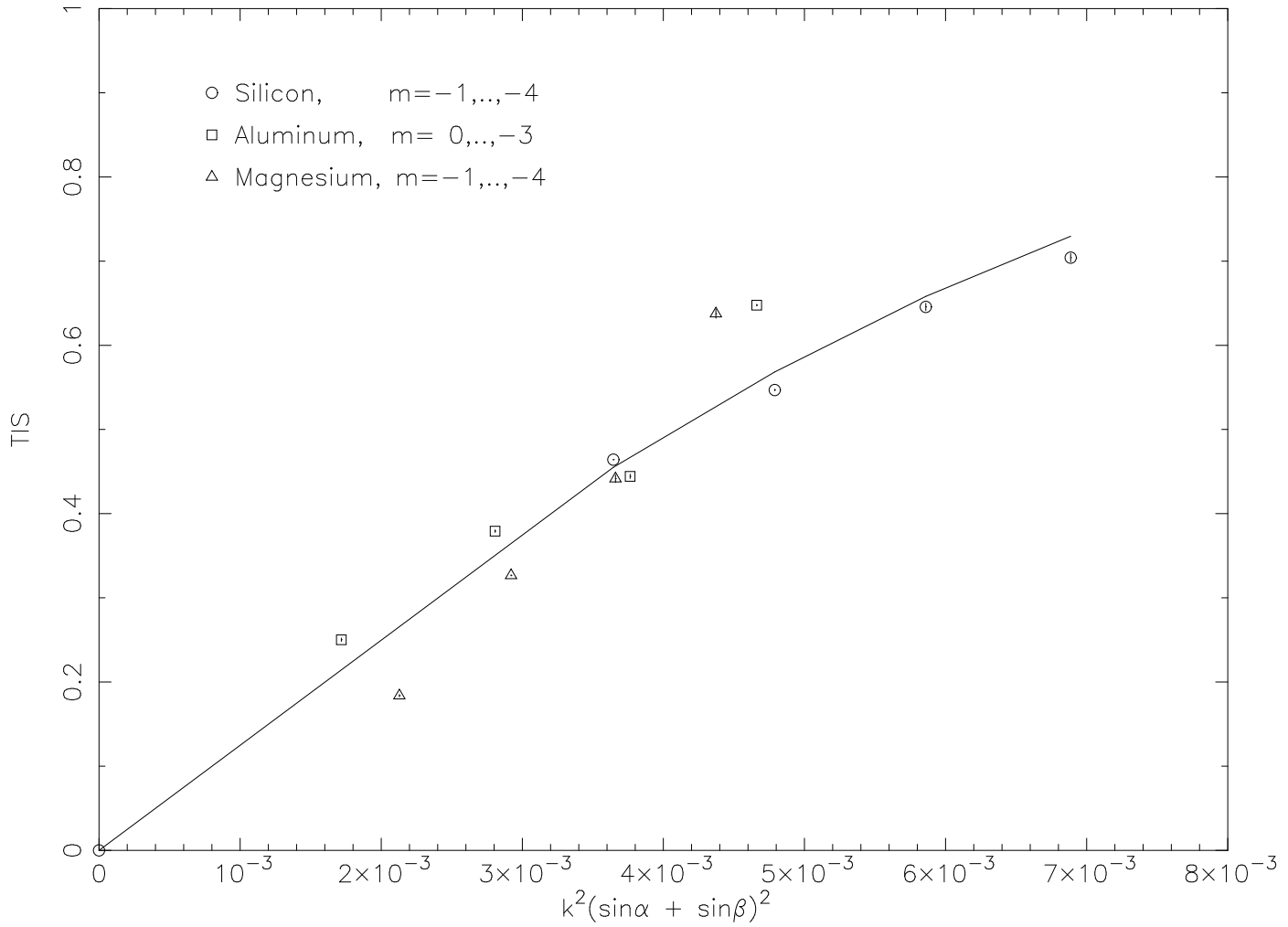


Figure 10: The total integrated scatter calculated from analyzing the Panter data of the three highest energy sources as in figure 9. The fitted curve is that of equation (6).

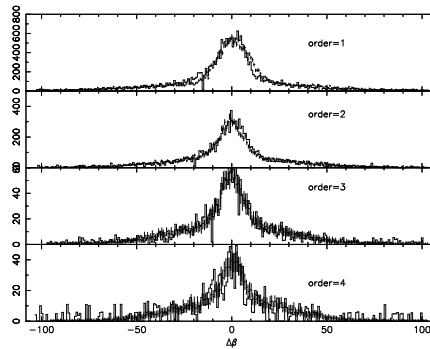


Figure 11: The same as figure 8 but with equation (6) used to calculate the total integrated scatter.